PCCP

Accepted Manuscript

This is an *Accepted Manuscript*, which has been through the Royal Society of Chemistry peer review process and has been accepted for publication.

Accepted Manuscripts are published online shortly after acceptance, before technical editing, formatting and proof reading. Using this free service, authors can make their results available to the community, in citable form, before we publish the edited article. We will replace this *Accepted Manuscript* with the edited and formatted *Advance Article* as soon as it is available.

You can find more information about *Accepted Manuscripts* in the Information for Authors.

Please note that technical editing may introduce minor changes to the text and/or graphics, which may alter content. The journal's standard Terms & Conditions and the Ethical guidelines still apply. In no event shall the Royal Society of Chemistry be held responsible for any errors or omissions in this *Accepted Manuscript* or any consequences arising from the use of any information it contains.

PCCP

ARTICLE TYPE

Oxygen vacancy assisted multiferroic property of Cu doped ZnO film

Hongyan Liu*, Yonglin Wang, Jianhua Wu, Guanli Zhang, Yue Yan*

5 Exploring multi-functional properties in a single material is the focus for future material design and applications. In this paper, we investigated the multiferroic property of Cu doped ZnO film using a combination of X-ray diffraction (XRD), transmission electron microscopy (TEM), X-ray absorption spectroscopy (XAS), classical magnetometry and electric measurements. The results show that the texture of Cu doped ZnO is deteriorated with increase in Cu contents, whereas the dielectric property is improved 10 due to the introduction of Cu ions. The XAS result reveals that the Cu atoms occupy the substitutional Zn sites in the ZnO host, and thus induce local electric dipoles owing to the displacement of Cu-O bond. The presence of oxygen vacancies together with Cu ions facilitates the movement of ferroelectric domain boundary, and contributes to the ferromagnetism due to the indirect exchange between Cu atoms and large-sized vacancy orbitals. The Cu dopped ZnO film is feasible for promising applications in 15 multiferroic devices.

1. Introduction

With rapid development of the semiconductor industry, a significant improvement in higher usage of a single material is the dominant goal for future material investigations. Exploring a 20 single material with various properties simultaneously, such as ferromagnetism, ferroelectricity, resistance switching, etc., is a viable method. Recently, there are tremendous research interests in multiferroic materials that simultaneously display magnetic and dipolar electrical orderings to construct new paradigms of 25 spintronics devices and data storage applications for higher memory density and energy efficiency.[1] Much of the recent works about multiferroic materials was mainly focused on silicon incompatible perovskite materials,[1] which are structurally complicated and difficult to synthesize, hence, limit their 30 multifunctional applications. It is urgent to explore a single material with silicon compatibility, which can be easily used in semiconductor industry.

Zinc oxide (ZnO), a wurtzite structure with space group of $P6_3mc$, has been of growing technological importance and has 35 received tremendous attention due to its versatile physical and chemical attributes.[2] ZnO is a well-known piezoelectric and photonic semiconductor with a wide band gap of 3.37 eV and a large exciton binding energy of 60 meV at room temperature, and it exhibits the largest piezoelectric response amongst the known 40 tetrahedral semiconductors.[3] Consequently, it is used extensively in such diverse areas as spintronic devices,[4] surface acoustic wave devices,[5] transparent conducting films,[6] gas sensors,[7] photocatalysts,[8] resistive random access memories,[9, 10] solar cells,[11] etc. More importantly, high quality ZnO film with tunable 45 properties, such as resistivity, electromechanical response, optical band gap, magnetism, etc., can be easily obtained by using various growing and doping methods.[12-14] Taping into its intriguing properties in ZnO films, it is technologically desirable to develop a single phase ZnO film with coexistence of 50 ferroelectricity and ferromagnetism. In the past, a number of reports have shown room temperature (RT) ferromagnetism in

ZnO films with low resistivity by substituting other transition-metal ions into Zn sites,[15] while several experiments have been designed to explore the ferroelectric-like behavior in doped bulk 55 crystals and ZnO films with high resistivity, and some of doped ZnO films indeed exhibit ferroelectricity.[16-19] Recently, some reports have shown the coexistence of ferroelectricity and ferromagnetism in doped ZnO thin films.[20-22] Despite the success in obtaining mutiferroic property in single phase ZnO film, the 60 underlying mechanism is not very clear, and the performance of mutiferroic films needs further improvement due to the insufficient insulating property, which hinders the ferroelectric measurement.

In this paper, we used Cu metal as dopant to study the 65 multiferroic property of ZnO film because (i) the radii of Cu^{2+} and Cu^{1+} ions are smaller than that of Zn^{2+} ion. The discrepancy in ions radius can induce local displacement in tetrahedrons when occupying the substitutional Zn sites, which will facilitate the inversion of ferroelectric domains. (ii) Cu atoms are well-known 70 as electron traps which results in a high resistivity film regardless of the presence of oxygen vacancy needed for ferromagnetism. After substituting for Zn, the bonding electrons are itinerant within the Cu_{Zn}-O bond due to the strong covalence, which will induce an electron deficiency in the neighboring Zn-O bonds.[23] A 75 higher resistivity of ZnO film is favorable for ferroelectric measurement. (iii) Neither metallic Cu nor its oxides (CuO and Cu_2O) are ferromagnetic at room-temperature, ruling out the possibility of ferromagnetism arising from the precipitates or the secondary phase. Cu doped ZnO film is reported to exhibit RT 80 ferromagnetism.[24, 25]

The aim of this study is threefold. First, we wanted to study the structural evolution of ZnO films as a function of Cu contents. A series of Cu doped ZnO films were deposited on $Pt(111)/Ti/SiO_2/Si(100)$ substrates using radio frequency reactive 85 magnetron sputtering, after which the structure was studied by X-ray diffraction (XRD) and transmission electron microscopy (TEM). Second, the local structure around specific atoms was

investigated with synchrotron based X-ray absorption spectroscopy (XAS), from which the exact bond length was extracted. Last, the ferroelectricity and ferromagnetism were measured and the underlying mechanism was discussed. The incorporation of Cu atoms and the presence of oxygen vacancy in ZnO film are two important factors for the multiferroic property.

2 Experimental

2.1 Preparation of ZnO films.

A series of Cu:ZnO films with various Cu contents were deposited on Pt(111)/Ti/SiO$_2$/Si(100) substrates at 350°C within a mixture of pure argon (99.999%) and oxygen (99.999%) gases by using radio frequency (RF) reactive magnetron co-sputtering method. The sputter chamber was equipped with three 3 inch sputter sources which were arranged confocally to enable co-sputtering of a variety of different composition films onto a rotating substrate. The target materials were copper and zinc with purity of 99.999%. The copper concentrations in the films were controlled by varying copper target power from 0 W to 13 W while keeping the zinc target power at 100 W using direct current (DC) and radio frequency (RF), respectively. The sputtering chamber was generally pumped down to a base pressure of 3×10^{-5} Pa, and then high purity argon and oxygen gases were introduced into the chamber with partial pressure of 0.6 Pa and 0.2 Pa, respectively. Prior to each film deposition, the target was cleaned *in situ* by Ar+ ion bombardment for 10 min and then pre-sputtered at the deposition conditions for 5 min, during which the substrates were covered by a rotatable shutter. For electrical measurements, Pt top electrodes with a thickness of 250 nm and a diameter of 300 μm were deposited on the as-prepared pure ZnO and Cu doped ZnO films using a shadow mask to form a metal-insulator-metal capacitor. The thickness of all film is about 250 nm, which was measured by a stylus profilometer (Dektak XT).

2.2 Characterizations of as-prepared ZnO films.

The structures of the Cu:ZnO films were analyzed by X-ray diffraction (XRD) using Cu-$K\alpha$ (λ=1.5406Å) radiation (Rigaku Smartlab) with Bragg-Brentano geometry. Transmission electron microscopy (TEM) studies were conducted on cross-sectional specimens in order to analyze the Cu:ZnO film microstructure in detail. TEM was performed on a JEOL 2010F operated at an accelerating voltage of 200 kV equipped with a double-tilt stage. Synchrotron radiation X-ray absorption spectroscopy (XAS) was used to obtain local structural information around specific elements. X-ray absorption spectroscopy measurements were carried out at beamline 14W1 of the Shanghai Synchrotron Radiation Facility (SSRF, Shanghai, China), operating at an electron beam energy of 3.5 GeV with a maximum current of *ca*. 210mA. A Si (111) double-crystal monochromator was used to select the X-ray energies, and a pair of vertically focusing Si mirrors was employed to suppress the high harmonics. XAS signals were collected in total fluorescence yield (TFY) mode both at the Cu K-edge (8978.9 eV) and the Zn K-edge (9658.6 eV), and the fluorescence intensity was recorded by a 13-element Ge detector at 90 ° with respect to the X-ray beam path. A reference standard metal foil of either copper or zinc was employed for each energy calibration. Each sample was oriented in a specific way to avoid the Bragg condition as much as possible. Subsequently, the experimental X-ray absorption data were processed using standard procedures with IFEFFIT software package.[26] The FEFF simulations were performed wherever necessary using IFEFFIT software package. The Cu content and

valence states along with oxygen vacancy in the samples were evaluated via Escalab 250Xi X-ray photoelectron spectrometer(XPS) with Al K_a radiation of 1486.6 eV. Prior to each XPS measurement, the sample was etched by Ar$^+$ ions sputtering for 5 min to avoid surface contamination. All of the spectra were calibrated with C 1s at 284.5 eV originating from adventitious carbon contamination. Besides, the Raman spectroscopy was also employed to further assess the oxygen vacancy in ZnO films. Ferroelectric properties including polarization-electric field (*P-E*) and leakage current density-voltage (*J-V*) characteristics were investigated with a TF Analyzer 2000 system. Magnetization measurements were performed in a superconducting quantum interference device (SQUID) magnetometer at room temperature (RT). The Cu doped ZnO films do not have sufficient conductivity to measure electrical parameters by Hall measurement.

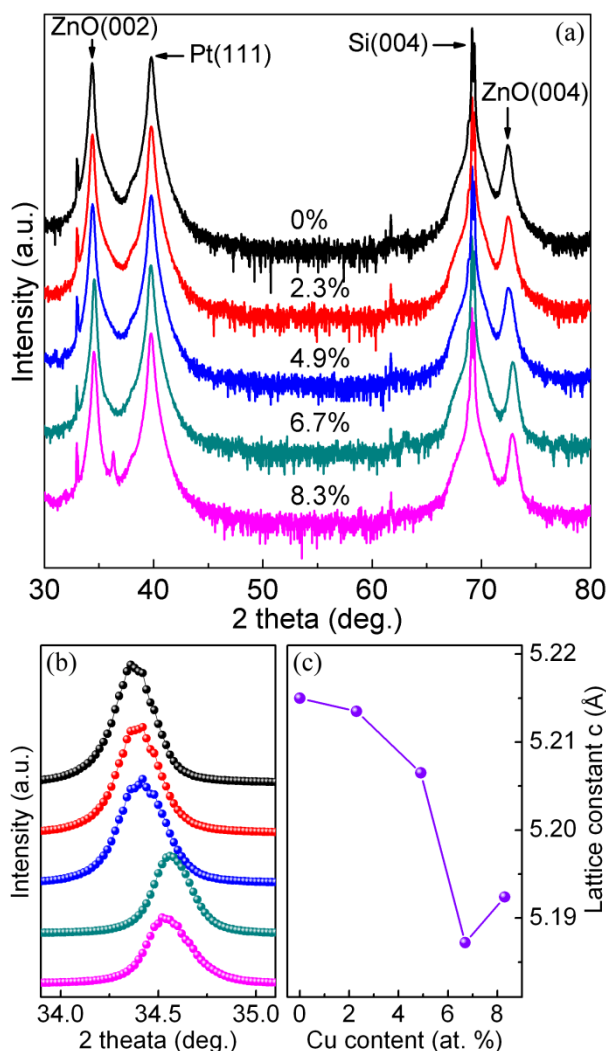## 3. Results and discussion

3.1 Structural characterizations

Figure 1. (color online) (a) θ-2θ XRD patterns of Cu$_x$Zn$_{1-x}$O (x=0, 0.023, 0.049, 0.067 and 0.083) films with intensities displayed on a logarithmic scale. The patterns are shifted vertically for clarity. (b) Enlarged view of the XRD spectra of ZnO (0002) plane in θ-2θ scan mode showing angular shift clearly with Cu concentration. (c) The lattice constant c of Cu$_x$Zn$_{1-x}$O as a function of Cu content x.

Fig. 1(a) displays the θ-2θ XRD spectra of $Cu_xZn_{1-x}O$ (x=0, 0.023, 0.049, 0.067 and 0.083) films. It clearly shows that, besides the peaks from Pt (111) and Si (00l), all the diffraction peaks correspond well to the standard diffraction patterns of wurtzite
5   ZnO with absence of any other peaks from Cu clusters or Cu oxides, indicative of the perfect incorporation of Cu atoms into the ZnO host lattice. Besides, the intensity of the ZnO (002) peak decreases, while peaks from ZnO (101) planes are accompanied with increasing Cu contents, indicating that the incorporation of
10 Cu ions into the ZnO host deteriorates the film crystal perfection. Moreover, a shift of ZnO (002) peaks toward higher angle side can be observed obviously upon Cu doping (shown in Fig. 1(b)), which suggests a contraction of the c lattice due to the incorporation of Cu atoms into ZnO host. The stress induced (002)
15 peak position shift can be ruled out considering the thicknesses of ZnO films, since a full relaxation of the epitaxial strain already occurs after a few atomic layers. Fig. 1(c) depicts the plot of c constant as a function of Cu content in ZnO films, which were calculated according to the relation $c=\lambda/\sin(\theta)$, where λ is the
20 wavelength of Cu radiate, θ is the diffraction peak position of (002) planes. It displays more clearly that a decrease of c constants appears after incorporation of Cu atoms. However, the 2θ position of ZnO (002) planes shifts reversely to lower angle side as the Cu content exceeds 6.7 at. %, and the tendency of the
25 c constant versus Cu content x relationship deviates from the empirical linear relationship predicted by the Vegard's law. The c lattice contraction can be easily understood considering the relevant ionic radii of Cu^+(0.60Å), Cu^{2+}(0.59Å) and Zn^{2+}(0.74Å).[27] Accordingly, substitution of Cu ions for Zn ions is
30 expected to induce lattice contraction due to the shorter interatomic distance of Cu_{Zn}-O bonds. For the abnormal increase in c constant with excess Cu incorporation such as for $Cu_{0.083}Zn_{0.917}O$ film, it is unclear why is so, and the likely cause may be the enclosure formation of CuO in ZnO matrix.
35   TEM observations were performed to characterize the microstructure and to investigate the possibility of presence of Cu metal or Cu related oxide clusters in the ZnO film. Fig. 2(a) shows a representative low magnification cross-sectional TEM image of $Cu_{0.067}Zn_{0.933}O$ film grown on Pt(111)/Ti/SiO$_2$/Si(100)
40 substrate, which exhibits a columnar structure with high c-axis preferential orientation. All the crystal grains with crystal size of from $ca.$ 40 nm to 100 nm are perpendicular to the substrate surface, penetrating through the entire film thickness. A high resolution TEM image (HRTEM) was shown in Fig. 2(b), in
45 which a prominent grain boundary was marked by an arrow. The inter-planar spacing of $Cu_{0.067}Zn_{0.933}O$ film is 0.5187 nm, which is in good agreement with that of XRD result. There were no observations of the presence of Cu metals or Cu related oxide clusters even though some lattice distortion or damage was
50 discernible in the HRTEM image. Fig. 2(c) exhibits the Fast Fourier Transform (FFT) along the [002] zone axis corresponding to the square area enclosed by a dashed box in Fig. 2(b). The FFT pattern corresponds well with that of wurtzite ZnO structure, and shows absence of spots from any secondary phase or precipitation,
55 which rules out the possibility of impurity phases, and further justifies the incorporation of Cu atoms into the ZnO lattice. Moreover, the interface between the Cu doped ZnO film and the substrate surface is atomically sharp with absence of any interface reaction or amorphous oxides as revealed in Fig. 2(d),
60 which somewhat reveals the local epitaxial growth of ZnO film on Pt surface. This growth model also facilitates the formation of c-axis oriented texture of Cu doped ZnO films.
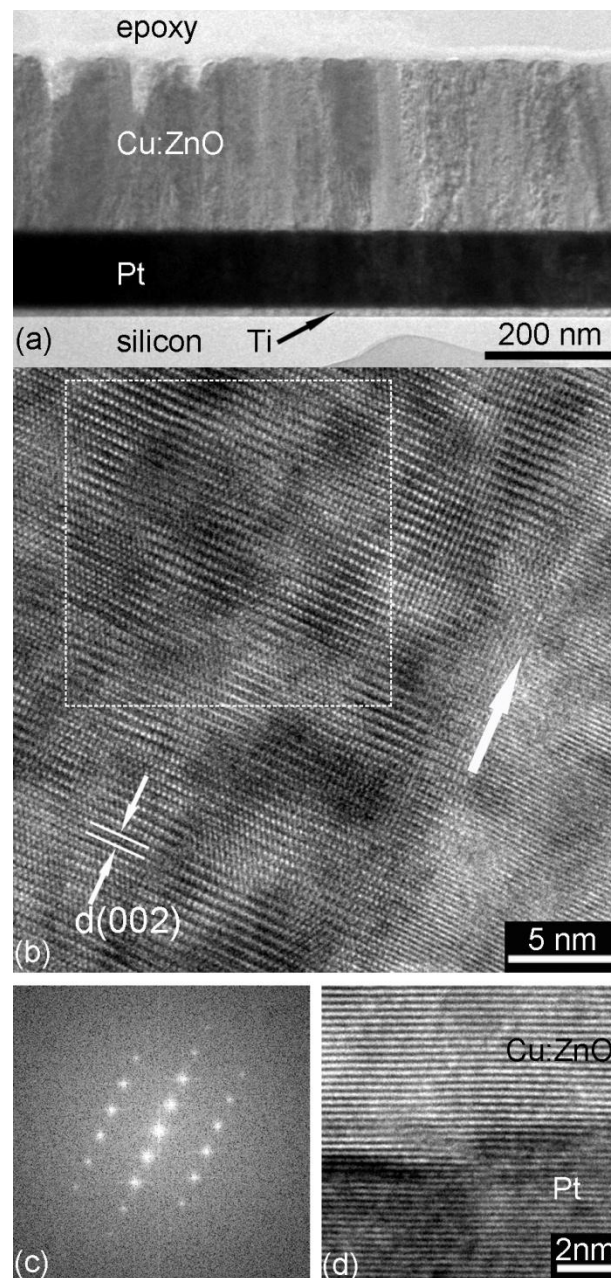
3.2 *J-V* characterizations

65

Figure 2. (a) Low magnification image of the cross-sectional sample of $Cu_{0.067}Zn_{0.933}O$ film. (b) HRTEM image of cross section of $Cu_{0.067}Zn_{0.933}O$ film showing a distinct grain boundary. (c) Fast Fourier Transform (FFT)
70 along the [002] zone axis corresponding to the square area enclosed by a dashed box in (b). (d) HRTEM image of the interface between Pt and $Cu_{0.067}Zn_{0.933}O$ film.

Since a highly resistive film with low leakage current is favorable
75 for the ferroelectric measurement to evaluate the feasibility of Cu doped ZnO film as a mutiferroic material, it is of vital importance to understand the conduction mechanism of the ferroelectric layer.
   Fig. 3 depicts the Cu content dependence of *J-V* characteristics of $Cu_xZn_{1-x}O$ films measured at room temperature with current
80 density shown on a logarithmic scale. It can be seen clearly that the leakage current diminishes drastically with increase in Cu contents in ZnO films. The ZnO film doped with 6.7 at.% Cu had the smallest leakage current, six orders of magnitude less than that of pure ZnO film. On the other hand, the leakage current
85 increases with further increase in Cu contents. The decrease of leakage current might be attributed to the incorporation of Cu

impurity with deep acceptor levels and electron-trap states in ZnO films, whereas the increase in leakage current accompanying higher Cu content might be due to the deterioration of crystal perfection. XRD results reveals that the textures of high Cu
5 concentrated ZnO films get weaker and the interstitial occupation emerges with further increase in Cu content, thus, lead to a higher density of defects and grain boundaries accompanied by higher density of carrier traps. Accordingly, a higher leakage current inevitably occurs.

10
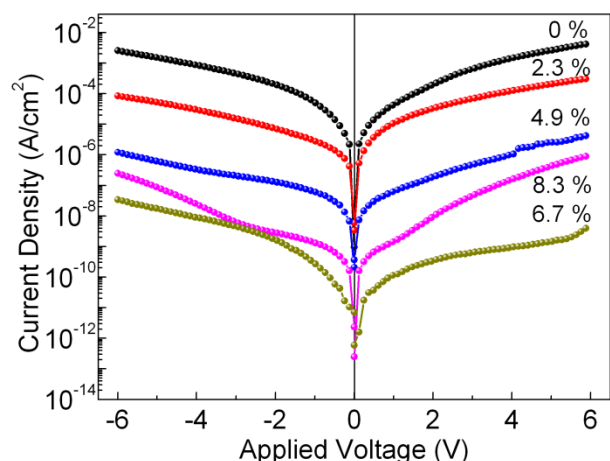
Figure 3. (color online) Cu content dependence of *J-V* characteristics of $Cu_xZn_{1-x}O$ films measured at room temperature. The current density is shown on a logarithmic scale.

15

3.3 Local structures

After experimenting with different samples, it was found that the $Cu_{0.067}Zn_{0.933}O$ film shows a good multiferroic behavior owing to
20 its considerably high resistivity and ferromagnetism (shown below). The $Cu_{0.067}Zn_{0.933}O$ film was selected as a representative sample to investigate the underlying mechanism of the multiferroic property in detail. Firstly, XAS measurements, including X-ray absorption near-edge structure (XANES) and
25 extended X-ray absorption fine structure (EXAFS), were performed to investigate the local structure around Cu and Zn atoms independently, from which the bond distances can be extracted. Fig. 4(a) displays the subtracted and normalized Zn *K*-edge XANES spectra of pure ZnO film and of $Cu_{0.067}Zn_{0.933}O$
30 film. As expected, the XANES spectrum of $Cu_{0.067}Zn_{0.933}O$ film features roughly the identical *c*-axis oriented ZnO structural profile as that of pure ZnO film, indicating that the Zn atoms are predominantly present in a divalent oxidation state occupying the center of tetrahedral configuration. The main peak located at *ca.*
35 9669.5 eV along with a shoulder at *ca.* 9664.5 eV, corresponding to the two peaks at *ca.* 9667.5 eV and *ca.* 9664.5 eV in the first derivatives, can be attributed to the Zn^{2+} dipole allowed electron transitions of 1*s*-4 p_π (along the *c*-axis) and 1*s*-4p_σ (in-plane), respectively.[28-30] The shoulder above the absorption edge at *ca.*
40 9680 eV is related to scattering contribution from high coordination shells.[31] Upon copper incorporation, the main peak at *ca.* 9669.5 eV is broadened compared with that of pure ZnO film as shown clearly in the inset to Fig. 4(a). This change is likely the result of Cu ions occupying the Zn sites, leading to the
45 reduction of long-range order. Except for this small disparity, the resemblance of the rest of XANES spectra indicates that the incorporation of Cu atoms only exert slight influence on the band structure of the ZnO host and the ZnO phase remains exactly the same structure.
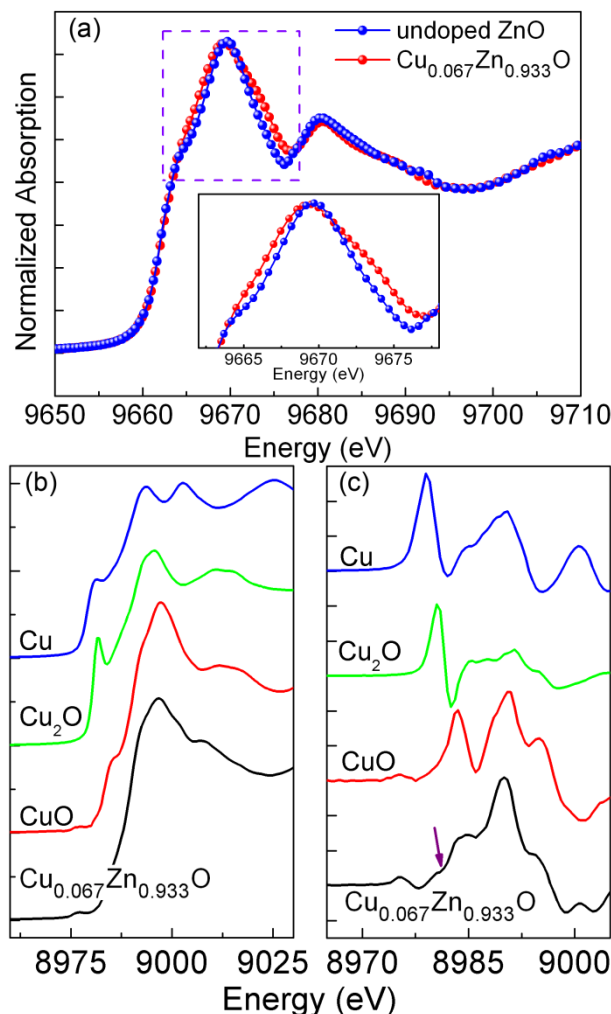
50

Figure 4. (color online) (a) Zn *K*-edge XANES spectra of pure ZnO film and of $Cu_{0.067}Zn_{0.933}O$ film. The inset shows the enlarged spectra of the peaks enclosed by dashed box. (b) Cu *K*-edge XANES spectra and (c) the
55 first derivatives of $Cu_{0.067}Zn_{0.933}O$ film and of bulk Cu, CuO and Cu_2O. The spectra are shifted vertically for clarity.

Fig. 4(b) and (c) depict the Cu *K*-edge XANES spectrum and the corresponding first derivative of $Cu_{0.067}Zn_{0.933}O$ film,
60 respectively, together with that of bulk Cu, CuO and Cu_2O for comparison. A tiny pre-edge peak located at *ca.* 8977.5 eV can be seen in Fig. 4(b), which is more pronounced in the first derivative plots as shown in Fig. 4(c). This feature is due to the quadrupole 1*s*-3*d* allowed pre-edge transition, which is generally present in
65 all Cu^{2+} compounds where the empty d states are available such as in the $3d^9$ electronic configuration of the Cu^{2+} ion occupying the center in a noncentrosymmetric environment.[32] Accordingly, some Cu ions with divalent state exist in the $Cu_{0.067}Zn_{0.933}O$ film. Other than this, a very weak shoulder centered at *ca.* 8981 eV
70 (indicted by an arrow) can be observed, which is shifted upward by 0.5 eV in comparison with that of Cu_2O (8980.5 eV). This weak shoulder is ascribed to the dipole allowed 1*s*-4*p* transition of Cu^{1+} in Cu_2O, indicating that a small part of the copper exists as Cu^{1+} state. Hence, it can be concluded that the Cu ions in the
75 samples are of two valence states, i.e., the coexistence of Cu^{2+} and Cu^{1+}.

In order to study the local atomic structure of the ZnO matrix in more detail, we performed extended X-ray absorption fine structure (EXAFS) measurements at the Zn and Cu *K*-edges,
80 respectively. The spectra were simulated with the FEFF 8.0

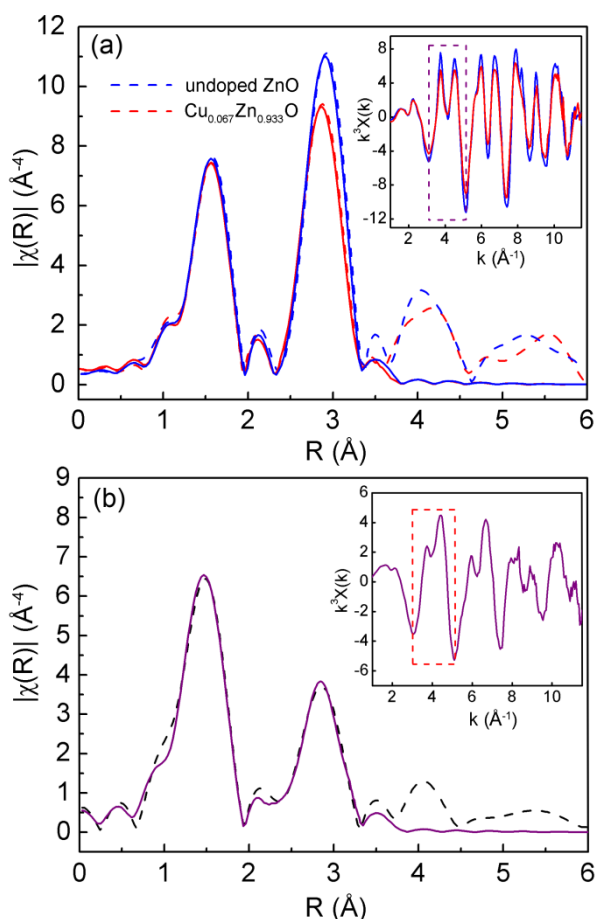Figure 5. (color online) Fourier transforms of the Zn K-edge (a) and Cu K-edge (b) k^3-weighted EXAFS spectra. Dased lines are the experimental data, and the solid lines are the simulations. Insets to the figures show the corresponding EXAFS oscillations. The dashed boxes enclose a feature that is characteristic of the ZnO structure.

software package. For the $Cu_{0.067}Zn_{0.933}O$ film, the Cu atoms are presumed to substitute for the Zn^{2+} sites as a wurtzite $Cu_{Zn}O$ cluster in ZnO film. The Fourier transforms (FT) of the Zn K-edge k^3-weighted EXAFS spectra together with the fitting curves are illustrated in Fig. 5(a). The inset to Fig. 5(a) displays the corresponding EXAFS oscillations, in which the profile enclosed by a dashed frame shows a feature that is characteristic of the ZnO structure. It can be seen obviously that the Fourier transform as well as the oscillation for the $Cu_{0.067}Zn_{0.933}O$ film features the identical profile as that of pure ZnO film, and the FEFF 8.0 simulation was excellent, which justifies the fact directly that Cu atoms occupy Zn^{2+} sites in the ZnO lattice without pronounced distortions in the ZnO host. In addition, the magnitude of the Fourier transform in the second peak for the $Cu_{0.067}Zn_{0.933}O$ film diminishes slightly in comparison with that of pure ZnO film, demonstrating that the crystal quality was deteriorated after incorporation of Cu dopant.

Fig. 5(b) shows the Fourier transform of Cu K-edge k^3-weighted EXAFS together with its best fit, and the corresponding EXAFS oscillation is also shown in the inset to Fig. 5(b). At a first glance, the spectral profile of Cu K-edge k^3-weighted EXAFS displays a good resemblance with that of Zn K-edge k^3-weighted EXAFS, which indicates that the microstructures around Zn and Cu atoms are similar From the Fourier transform of the Cu K-edge k^3-weighted EXAFS spectrum (Fig. 5(b)), two major peaks can be observed at $ca.$ 1.41 Å and $ca.$ 2.87 Å, which

Table 1. Structural parameters of Zn and Cu K-edge EXAFS refinements

sample	element	Shell	N	R(Å)	$2\sigma^2$(Å^2)
ZnO	Zn	Zn-O	4.01	1.972	0.0052
		Zn-Zn	11.3	3.22	0.011
$Cu_{0.067}Zn_{0.933}O$	Cu	Cu-O	3.98	1.967	0.0064
		Cu-Zn	11.1	3.17	0.012

N = number of atoms in the different shells. R = radial distance of atoms. $2\sigma^2$ = Debye-Waller term (with σ^2 = Debye-Waller factor)

correspond to the Cu-O and Cu-Zn interaction, respectively.

The structural parameters extracted from FEFF 8.0 simulations are compiled in Table 1. From the results, one can see that the pure ZnO film possesses the similar structural characters as that of wurtzite ZnO, namely, with Zn-O bond length of 1.972 Å in the first shell and with coordination number of 4.0 around Zn atoms. In the case of $Cu_{0.067}Zn_{0.933}O$ film, the coordination number and the Zn-O bond like Cu-O bond length decrease to 3.98 and 1.967 Å, respectively. The second shell interatomic distance also decreases from 3.22 Å for undoped ZnO film to 3.17 Å for $Cu_{0.067}Zn_{0.933}O$ film. The contraction in bond length of both the first and second shell is due to the ionic radius discrepancy between Cu and Zn ions. These results indicate that Cu atoms are occupying the Zn sites substitutionally in the hexagonal host lattice without pronounced distortions in the interatomic distances of the two nearest neighbor shells.
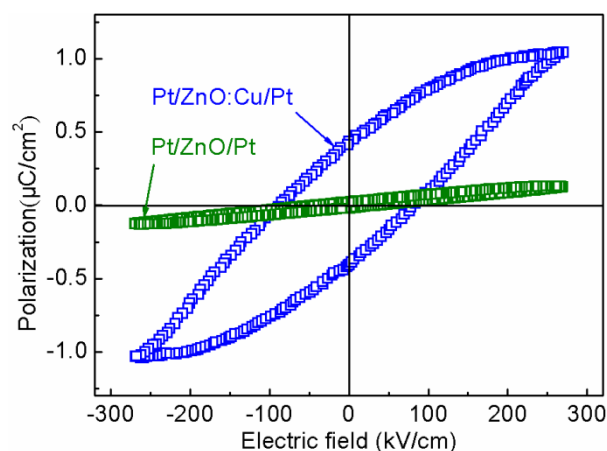
3.4 Ferroelectric and magnetic properties

Figure 6. (color online) P-E characteristic of $Cu_{0.067}Zn_{0.933}O$ film together with undoped ZnO film measured with frequency of 0.5 kHz at room temperature.

Fig. 6 shows the room temperature polarization-applied electric field (P-E) characteristic of $Cu_{0.067}Zn_{0.933}O$ film with a comparison to that of undoped ZnO film measured with 0.5 kHz. As shown in the figure, the P-E curve of $Cu_{0.067}Zn_{0.933}O$ film displays well-defined hysteresis loop, while no hysteresis loop can be observed in P-E curve of undoped ZnO film, which is completely linear. Additionally, both of the coercive field and the remanent polarization only decrease slightly with increase in the measurement frequency (the curves are not shown here). These results indicate that the resistivity of $Cu_{0.067}Zn_{0.933}O$ film is sufficient for the measurement of ferroelectricity, which might be viable to serve as a multiferroic material. The presence of ferroelectricity in $Cu_{0.067}Zn_{0.933}O$ film is attributed to the substitution of smaller Cu^{2+} ions (0.59 Å) and/or Cu^{1+} ions (0.6 Å) for Zn^{2+} (0.74 Å), together with the assistance of oxygen vacancy. As extracted from the EXAFS measurement, the local bond length around metal atoms reduces from 1.972 Å for Zn-O to

1.967 Å for Cu-O bond after incorporation of Cu atoms into ZnO host. As a result, the local CuO_4 tetrahedron constriction and Cu^{2+} and/or Cu^{1+} displacement was induced. Moreover, oxygen vacancies are expected to play a critical role in polarization

5 switching.[33] The presence of oxygen vacancy is attested by the XPS spectrum (shown in Fig. 8 and discussed below). Due to the presence of oxygen vacancy, the Cu atom lost its bonding to the missing oxygen, thus, the Cu atom displaces more severely and the Cu-O bond rotates more freely under external electric field. It

10 is therefore conclude that the displacement of the smaller substitutional Cu^{2+} and/or Cu^{1+} ions, which occupy off-center positions of the ZnO tetrahedrons inducing local electric dipoles and spontaneous polarizations, and the presence of oxygen vacancy are responsible for the ferroelectricity in the

15 $Cu_{0.067}Zn_{0.933}O$ system.

Fig. 7 shows the room temperature magnetization-magnetic field (M-H) characteristics of $Cu_{0.067}Zn_{0.933}O$ film and of pure ZnO film. The background signals from the substrate and sample holder have been subtracted. From the figure, one can see that the

20 pure ZnO film shows a paramagnetic property, while the $Cu_{0.067}Zn_{0.933}O$ film displays a distinct room temperature ferromagnetic characteristic. In order to make clear the origin of the magnetism in the present case, we performed XPS at first to investigate the chemical valence states of Cu ions and the

25 possibility of oxygen vacancy in $Cu_{0.067}Zn_{0.933}O$ film.

Fig. 8(a) shows the XPS spectrum of the Cu $2p$ core level for $Cu_{0.067}Zn_{0.933}O$ film. The spectrum of Cu $2p$ core level XPS can be deconvoluted into two components of Cu^{2+} and Cu^{1+} by using Gaussian curve fitting. The fittings were accomplished by fixing

30 the $2p_{3/2}$ peak at 933.6 eV and $2p_{1/2}$ peak at 953.5 eV for Cu^{2+} and fixing the $2p_{3/2}$ peak at 932.6 eV and $2p_{1/2}$ peak at 952.5 eV for Cu^{1+}, respectively. It shows obviously that the Cu ions are of two valence states. Meanwhile, the XPS spectrum of O1s core level is also displayed in the inset to Fig. 8(a). The spectrum is fitted into

35 two components centered at *ca.* 530.27 eV and *ca.* 531.98 eV using two Gaussian curve fittings. The component at lower and higher binding energy side can be attributed to O^{2+} ions in wurtzite structure of hexagonal Zn^{2+} ions array and in the oxygen deficient regions within the matrix of ZnO, respectively. Due to

40 the lower formation energy of oxygen vacancies in oxides compared with cation interstitials,[34] one can conclude that the high oxygen deficiency in ZnO is attributed to oxygen vacancies instead of zinc interstitials. The presence of oxygen vacancy in ZnO can be further demonstrated by Raman spectrum, which is

45 shown in Fig. 8(b). Compared with the bare silicon substrate, a broad peak at *ca.* 585cm^{-1} in the Raman spectrum can be
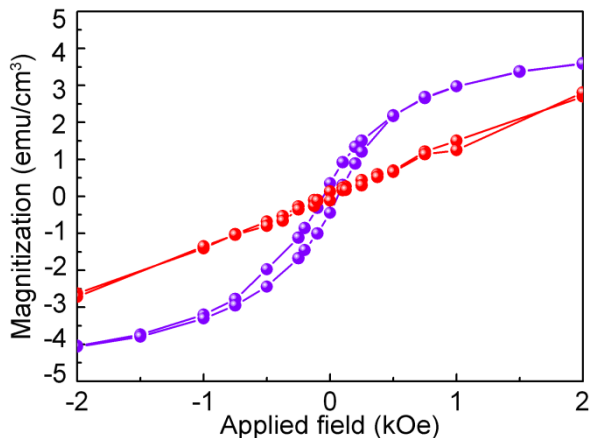

Figure. 7 (color online) Room temperature M-H curves of $Cu_{0.067}Zn_{0.933}O$
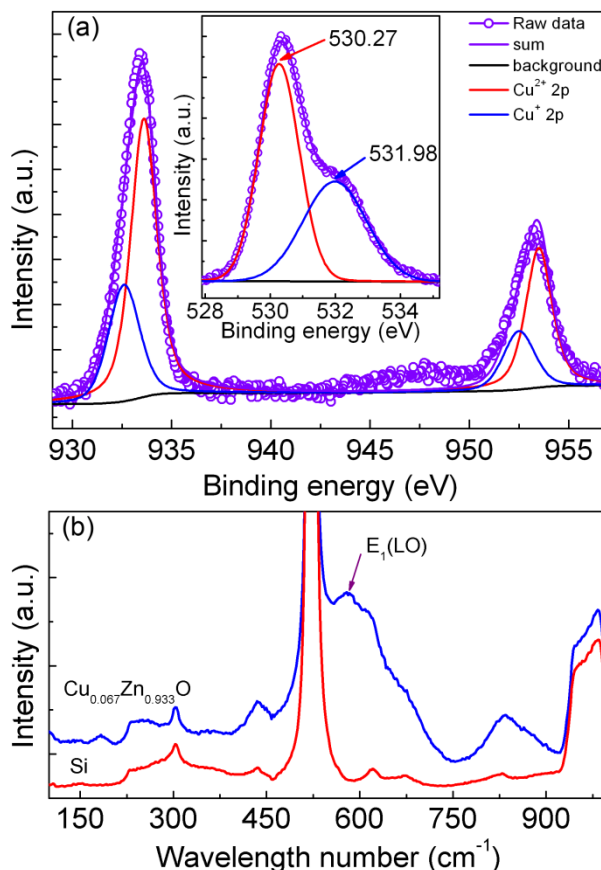50 film and of pure ZnO film.

Figure 8. (color online) (a) XPS spectrum of the Cu $2p$ core level for $Cu_{0.067}Zn_{0.933}O$ film, together with two corresponding Gaussian fittings. The inset to the figure shows the XPS spectrum of O 1s core level. (b)
55 Raman spectra of $Cu_{0.067}Zn_{0.933}O$ film and Si substrate.

observed obviously. This peak can be ascribed to the oxygen vacancy related E_1(LO) peak, indicative of the presence of oxygen vacancy in ZnO film.[22] Eventhough the presence of
60 oxygen vacancy in pure ZnO film, it is free of ferromagnetism as shown in Fig. 7. Hence, the origin of FTRM is not solely from oxygen vacancy. As discussed above, the Cu atoms occupy the center positions of tetrahedron, forming a strong covalent Cu_{Zn}-O bond, within which the bonding electrons are itinerant, making
65 the Cu ions carry a mixed d^9 and d^{10} character. Herng *et al.*[12] proposed that the origin of FTRM in copper doped ZnO films is due to the indirect exchange mechanism. They state that the alignments of localized large moments of Cu^{2+} in the vicinity of V_O are mediated by the large-sized vacancy orbitals, which
70 results in the long range ferromagnetic order. Considering the XPS analysis together with XAFS results, we can conclude that the origin of ferromagnetism in the present case is due to the indirect exchange mechanism. Besides, the bound magnetic polarons (BMP) proposed by Coey *et* al. is also legitimate for
75 explanation of RTFM in our Cu doped ZnO film.[35] We will thus argue that the covalent Cu_{Zn}-O bonds together with oxygen vacancies play an essential role in the establishment of the ferromagnetic ordering in Cu dopped ZnO film.

As discussed above, after introduction of Cu atoms in the ZnO
80 film, the texture of Cu doped ZnO film is degraded, while the dielectric property is improved. The Cu atoms occupy the substitutional Zn sites in the ZnO host, inducing local electric dipoles due to the displacement of Cu-O bond. The presence of oxygen vacancies together with Cu ions facilitates the movement
85 of ferroelectric domain boundary, and contributes to the

ferromagnetism due to the indirect exchange between Cu atoms and large-sized vacancy orbitals. As a result, the Cu dopped ZnO film may be a feasible promising candidate as a multiferroic material in applications in multiferroic devices.

Notes and references

Beijing Institute of Aeronautical Materials, Beijing, P.R. China, 100095. Fax:+86-10-62772907;Tel:+86-10-62497668;E-mail: lhy0207@126.com; yue.yan@biam.ac.cn

1   R. Ramesh and N. A. Spaldin, Nat. Mater., 2007, **6**, 21.
2   U. Özgür, Y. I. Alivov, C. Liu, A. Teke, M. A. Reshchikov, S. Doğan, V. Avrutin, S. J. Cho and H. Morkoç, J. Appl. Phys., 2005, **98**, 041301.
3   A. Dal Corso, M. Posternak, R. Resta and A. Baldereschi, Phys. Rev. B, 1994, **50**, 10715.
4   F. Pan, C. Song, X. J. Liu, Y. C. Yang and F. Zeng, Mater. Sci. Eng. R-Rep., 2008, **62**, 1.
5   J. T. Luo, F. Pan, P. Fan, F. Zeng, D. P. Zhang, Z. H. Zheng and G. X. Liang, Appl. Phys. Lett., 2012, **101**, 172909.
6   J. Sun, W. Yang, Y. Huang, W. Soon Lai, A. Lee, C. Fu Wang and H. Gong, J. Appl. Phys., 2012, **112**, 083709.
7   G. Qi, L. Zhang and Z. Yuan, Phys. Chem. Chem. Phys., 2014, **16**, 13434.
8   S. Kuriakose, B. Satpati and S. Mohapatra, Phys. Chem. Chem. Phys., 2014, **16**, 12741.
9   F. Pan, S. Gao, C. Chen, C. Song and F. Zeng, Materials Science and Engineering R, 2014, **83**, 1.
10 A. S. Zoolfakar, R. A. Kadir, R. A. Rani, S. Balendhran, X. Liu, E. Kats, S. K. Bhargava, M. Bhaskaran, S. Sriram, S. Zhuiykov, A. P. O'Mullane and K. Kalantar-zadeh, Phys. Chem. Chem. Phys., 2013, **15**, 10376.
11 R. Pipat, Y. Susumu and S. Takashi, Phys. Chem. Chem. Phys., 2013, **15**, 9516.
12 Y. C. Yang, C. Song, X. H. Wang, F. Zeng and F. Pan, Appl. Phys. Lett., 2008, **92**, 012907.
13 Y. Q. Chen, X. J. Zheng and X. Feng, Nanotechnology, 2010, **21**, 055708.
14 Y. G. Zhang, H. Y. He and B. C. Pan, Phys. Chem. Chem. Phys., 2013, **15**, 2932.
15 S. Mal, J. Appl. Phys., 2012, **112**, 113917.
16 C. C. Lin, C. C. Chang, C. J. Wu, Z. L. Tseng, J. F. Tang, S.Y. Chu, Y. C. Chen and X. Qi, Appl. Phys. Lett., 2013, **102**, 102107.
17 M. Joseph, H. Tabata and T. Kawai, Appl. Phys. Lett., 1999, **74**, 2534.
18 Y. C. Yang, C. Song, F. Zeng, F. Pan, Y. N. Xie and T. Liu, Appl. Phys. Lett., 2007, **90**, 242903.
19 M. K. Gupta and B. Kumar, J. Mater. Chem., 2011, **21**, 14559.
20 Y. C. Yang, C. F. Zhong, X. H. Wang, B. He, S. Q. Wei, F. Zeng and F. Pan, J. Appl. Phys., 2008, **104**, 064102.
21 C. W. Zou, H. J. Wang, M. L. Yin, M. Li, C. S. Liu, L. P. Guo, D. J. Fu and T. W. Kang, J. Cryst. Growth, 2010, **312**, 906.
22 T. S. Herng, M. F. Wong, D. Qi, J. Yi, A. Kumar, A. Huang, F. C. Kartawidjaja, S. Smadici, P. Abbamonte, C. Sánchez-Hanke, S. Shannigrahi, J. M. Xue, J. Wang, Y. P. Feng, A. Rusydi, K. Zeng and J. Ding, Adv. Mater., 2011, **23**, 1635.
23 Q. Ma, D. Buchholz and R. Chang, Phys. Rev. B, 2008, **78**, 214429.
24 T. Herng, D. C. Qi, T. Berlijn, J. Yi, K. Yang, Y. Dai, Y. Feng, I. Santoso, C. Sánchez-Hanke, X. Gao, A. Wee, W. Ku, J. Ding and A. Rusydi, Phys. Rev. Lett., 2010, **105**, 207201.
25 H. Liu, F. Zeng, S. Gao, G. Wang, C. Song and F. Pan, Phys. Chem. Chem. Phys., 2013, **15**, 13153.
26 B. Ravel and M. Newville, Journal of Synchrotron Radiation, 2005, **12**, 537.
27 R. Shannon, Acta Crystallographica Section A: Crystal Physics, Diffraction, Theoretical and General Crystallography, 1976, **32**, 751.
28 D. Grandjean, V. Pelipenko, E. D. Batyrev, J. C. van den Heuvel, A. A. Khassin, T. M. Yurieva and B. M. Weckhuysen, J. Phys. Chem. C, 2011, **115**, 20175.
29 J. Chiou, K. Kumar, J. Jan, H. Tsai, C. Bao, W.-F. Pong, F. Chien, M. H. Tsai, I. H. Hong and R. Klauser, Appl. Phys. Lett., 2004, **85**, 3220.
30 J. Haug, A. Chassé, M. Dubiel, C. Eisenschmidt, M. Khalid and P. Esquinazi, J. Appl. Phys., 2011, **110**, 063507.
31 T. Liu, H. Xu, W. S. Chin, Z. Yong and A. T. Wee, J. Phys. Chem. C, 2008, **112**, 3489.
32 Q. Ma, J.T. Prater, C. Sudakar, R. A. Rosenberg and J. Narayan, J. Phys.: Condens. Matter, 2012, 24, 306002.
33 T. S. Herng, A. Kumar, C. S. Ong, Y. P. Feng, Y. H. Lu, K. Y. Zeng and J. Ding, Scientific Reports, 2012, **2**, 587.
34 S. Lany and A. Zunger, Phys. Rev. Lett., 2007, **98**, 45501.
35 J. Coey, M. Venkatesan and C. Fitzgerald, Nature materials, 2005, **4**, 173.